Excess Water in Astronaut Helmet During EVA on ISS: Mitigations with Flight Demonstrations

Mark M. Weislogel[1], Oleg Krishcko[2] and Logan J. Torres[3]
IRPI LLC, Wilsonville, OR, 97070

Colin S. Campbell[4], Paul D. Dum[5], John C. Graf[6] and Tessa J. Rundle[7]
NASA Johnson Space Center, Houston, TX, 77058

Following a second crew report of excess water inexplicably accumulating in the helmet during EVA-80 on March 23, 2022, NASA initiated an aggressive effort to identify, mitigate, and/or eliminate all sources of the potentially life-threatening water. Our narration highlights demonstrations of microgravity flow expectations using terrestrial scale models, mitigations to dangerous water migration within the helmet, low-g two-phase flow separations for the flow entering the helmet, and an investigation of the nature of liquid carry-over from the EMU condensing heat exchanger source. Fast-to-flight demonstrations of each aspect of the work are carried out during hands-on crew interaction with flight scale hardware on ISS during the 2022-2023 timeframe. The results of the tests are described with a focus on the rarely observed, and thus rarely studied, large length scale air-driven wall-bound droplet and rivulet two-phase flows in microgravity. The success of the mitigations and directions for continued work is discussed in summary.

Nomenclature

1-g	=	acceleration due to gravity, 9.8 m/s^2	a	=	acceleration field strength (m/s^2)
a, l	=	subscripts for air, liquid	A	=	Cross-flow (section) area
A	=	effective cross section area	Bo	=	Bond Number, $\rho a \delta^2/\sigma$
CHX	=	Condensing Heat Exchanger	ConOps	=	Concept of Operations
D	=	characteristic diameter, droplet	low-g	=	low-gravity, << 1-g, microgravity
EGS	=	EMU Geometry Simulator	EHP	=	EVA and HSM Program
EMU	=	Extravehicular Mobility Unit	EVA	=	Extra-Vehicular Activity
FRR	=	Flexible Retention Reservoir	h	=	height
HAB	=	Helmet Absorption Band	HAP	=	Helmet Absorption Pad
HAP-E	=	Helmet Absorption Pad Extender	HSM	=	Human Surface Mobility
HUT	=	Hard Upper Torso	i	=	i^{th} Vent Pad Vent Duct
IVA	=	Intra-Vehicular Activity	l, L	=	length
MWA	=	Maintenance Work Area	NBL	=	Neutral Buoyancy Laboratory
OpNom	=	Operations Nomenclature	P	=	pressure

[1]Principal Engineer, 27501 SW 95th Ave., Ste 930.
[2]Engineer, 27501 SW 95th Ave., Ste 930.
[3]Sr. Engineer, 27501 SW 95th Ave., Ste 930.
[4]EVA Technology Development Lead, Space Suit and Crew Survival Branch, 2101 E. NASA Parkway, EC5.
[5]EVA Systems Group Lead, EVA Operations Branch, 2101 E. NASA Parkway, CX-351.
[6]Technology Development Lead for Life Support, 2101 E. NASA Parkway, EC3.
[7]Space Suit Development Engineer, Space Suit and Crew Survival Systems Branch, 2101 E. NASA Parkway, EC5.

Q	=	volumetric flow rate	Re	=	Reynolds Number, $\rho UD/\mu$
SLA	=	Stereolithography	T2CCS	=	T2 Condensate Capture System
TAVVID	=	T2 & Ventilation Visualization ISS Demonstration	t	=	time
TRL	=	Technology Readiness Level	U	=	fluid velocity
V	=	volume	w	=	width
We	=	Weber Number, $\rho U^2 D/\sigma$	δ	=	Vent Pad depth
θ	=	contact angle (equilibrium, advance, recede)	ρ	=	density
σ	=	surface tension	μ	=	dynamic viscosity

I. Abbreviated EMU/EVA Water Leak and Mitigations Story

A potentially catastrophic release of water into the helmet of ESA Astronaut Luca Parmitano[1] during EVA-23 occurred on July 16, 2013. A mishap investigation was immediately conducted by NASA resulting in several actions to reduce the chances of a future catastrophic 'water-in-helmet' event and mitigate the impacts if it did occur. Key items included water quality specifications and water quality monitoring, hardware in the helmet (Helmet Absorption Pad and Snorkel) and updated operational responses to enable faster and more optimized response if water was observed. At this time, it was acknowledged that sublimator carry-over could result in "small" amounts of water entering the helmet and this was accepted if it did not interfere with crew breathing or vision. Following EVA-80 March 23, 2022, ESA Astronaut Matthias Maurer[2] reported a similar, though lower volume, helmet water event. Due in part to the mounting occurrences, age of the suits, potential premature termination of EVAs, visibility and possible inhalation risks, NASA temporarily halted EVAs on ISS (announced May 17, 2022) and directly pursued a path to mitigate potentially critical or even catastrophic water release events within the suit. The investigation began internally April 18, 2022, with an exhaustive review of EMU water sources, with each addressed by mitigations. Potential solutions pursued received exhaustive flight certification attention prioritizing the safest, most minimal, most materially compatible, 'do-no-harm' concepts. In the process, NASA became open to solutions requiring some modification(s) to the suit. Initial considerations were restricted to the Helmet bubble but soon expanded upstream to include the T2 Port region, Vent Loop plumbing, and Sublimator Condensing Heat Exchanger (CHX) within the EMU. Due to the novelty of the flow phenomena present, we largely report the effort to date from a microgravity fluid physics challenges perspective.

For the most part, helmet water volumes beyond typical visor condensation have been observed and reported to NASA. Though the specific amounts have been difficult to estimate visually by both crew and ground teams, when observed and reported, free water volumes inside the helmet generally increase with increasing EVA duration and crew exertion. Water volumes observed and estimated as high as 1500 mL can be life-threatening[1]. Though a variety of water sources are present within the EMU[3], we address herein the significantly lower volume source of the Sublimator CHX of the EMU, which nonetheless provides ample free water to be of concern, < 360 mL. A simplified schematic of the EMU Sublimator CHX and downstream plumbing elements leading to and including the helmet is provided in Figure 1. Specific helmet details are provided in Figure 2 including an image of water in the helmet taken during follow-on tests performed on ISS[4].

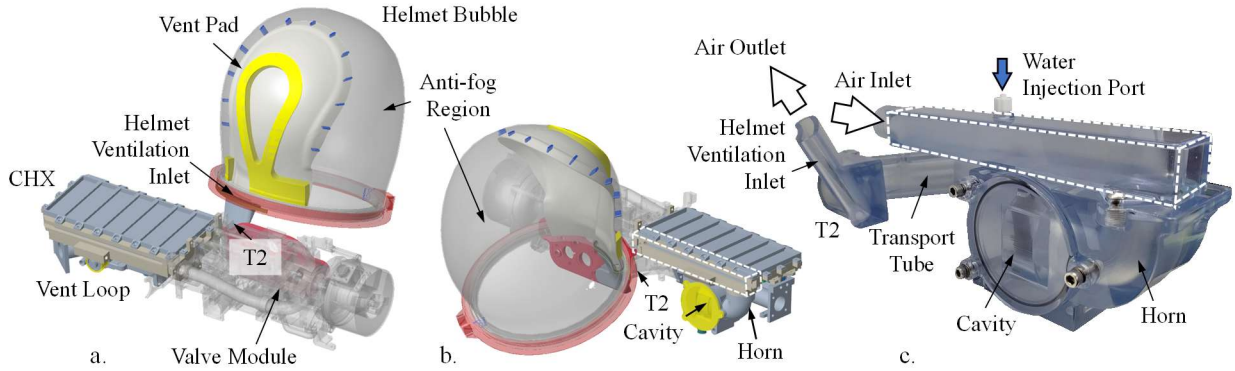

Figure 1. Simplified models of pertinent Helmet, T2 port region, and Vent Loop plumbing elements: a. rear view identifying Vent Loop and Valve Module (not addressed herein), b. front view with Sublimator CHX downstream manifold dashed in white, and c. 1:1 scale SLA EVA Geometry Simulator (EGS; aka Vent Loop model) demonstration model with model Sublimator CHX downstream manifold dashed in white.

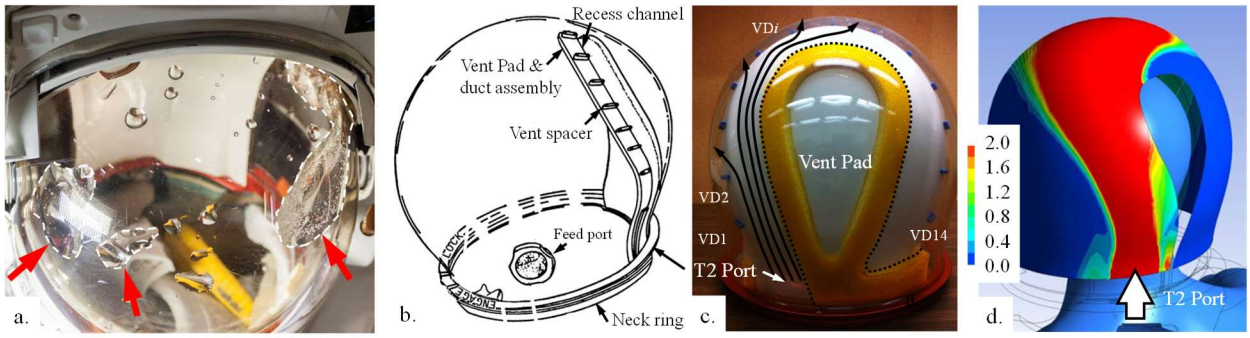

Figure 2. EMU Helmet: a. Helmet-bound water droplets with micro-bubble laden large volumes identified within white-dashed regions[4], b. labeled schematic identifying Vent Pad[5], c. rear view of Helmet identifying impermeable region of Vent Pad assembly (dotted line) and 14 Vent Ducts with notional streamlines (solid lines), and d. map of wall shear stress (in psi) from full-CFD simulations of single-phase airflow through T2 Port, Vent Ducts, and Helmet[12].

Figure 1 identifies the four regions investigated in reverse order of flow direction: (1) the Helmet, (2) T2 Port, and (3) Vent Loop, the latter which includes the assumed primary water source of the (4) EMU Sublimator CHX, downstream manifold, horn, disc valve cavity, and transport tubing just upstream of the T2 Port. In this paper, we first provide a description of the flow phenomena from a microgravity capillary fluidics perspective. We then briefly review the requirements imposed for the individual and combined 'helmet leak' mitigation investigations. We highlight the salient details of these three efforts supported by terrestrial research, summarizing each with discussions of either completed or scheduled flight demonstrations aboard ISS. We conclude with a discussion of the overall water mitigation performance of the fully integrated system: Helmet, T2 Port, and Vent Loop.

II. Description of the Flow: Sublimator, Vent Loop, T2 Port, Helmet

The EMUs were constructed by Hamilton Sundstrand/Collins Aerospace[5] circa 1975-1982. As a result, certain reverse engineering, re-analysis, and re-test efforts are necessary to determine the expected fluidic behavior of the aging systems because the original designers could not always be contacted, and thus their motives appreciated. The suits have logged more than 1000 EVA hours on the Space Shuttles and ISS. However, we are unaware of any investigation of the actual liquid transport within the system at prolonged microgravity conditions. Such an effort is briefly reported herein as a byproduct of the broader helmet water mitigation effort.

In short, as assumed, hold-up (i.e., 'trapped') condensate in the EMU Sublimator CHX is released from the device due to high condensate production activities, failing pinning edges, degraded hydrophilic coatings, perturbations introduced by crew motions, and IVA re-pressurization which results in increased gas density and inertial flow through the Sublimator. Due to the low liquid flow rate ratio, likely partial wetting conditions, and transitional Reynolds and Weber numbers[6,7] ($Re_D \sim O(2000)$, $We_D \sim O(4)$), condensate water released from the CHX becomes wall-bound droplets and rivulets that are driven downstream by the airflow only to hold-up to various degrees within the Vent Loop. Once a critical Vent Loop liquid hold-up volume is reached, further liquid introductions and crew motions are capable of releasing wall-bound droplets and rivulets and even transient liquid slugs and free droplets through the T2 Port and into the helmet. Such liquid is driven through and distributed by the vent pad tangentially along the inner surface of the helmet. If large enough $\gtrsim O(10$ mL), such helmet-bound droplets and rivulets can bridge and/or transfer passively to the head and/or face. Droplets and rivulets reaching the antifog region of the helmet dissolve the coating to various degrees and 'wet-out,' spreading in all directions along the helmet as a thick, potentially bubbly, mobile film. A representative illustration of these effects is provided in Figure 3. Our effort seeks to mitigate if not eliminate such occurrences. Insightful details of this process are provided below in the remainder in this section.

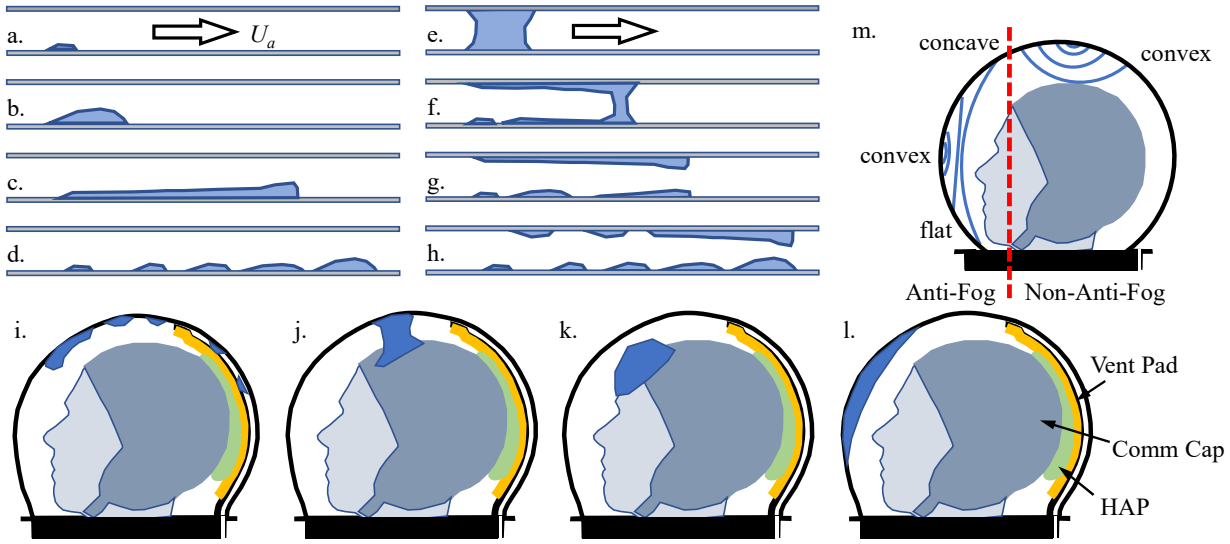

Figure 3. Collection of developing transient two-phase capillary flow expectations pertinent to Helmet: a.-h. train of wall-bound drops in a conduit from a single coalescing wall-bound drop (a.-d.) and a slug (e.-h.). Expectations in the helmet are shopwn in i., including a liquid bridge j. with transfer to head k., and transfer back to Helmet l. depending on anti-fog wetting conditions. Stable Helmet-bound drop configurations depending on local wetting and drop volume are shown in m. To be described shortly, the HAP is shown in green between Vent Pad and Comm Cap.

The Sublimator cold plate within the EMU provides 50 – 100 W nominal expected cooling, corresponding to 1.5 – 3.0 mL/min water condensate collection rates by the CHX from the suit-circulated humid air. The Sublimator CHX and portions of nearby conduit are coated with an approximately 50 – 150 μm thick ceramic-based film. The coating is hydrophilic, promoting nearly perfect wetting of the doubly-sinusoidal approximately 50 – 75 μm thick aluminum fin stock at the time of application (as many as 16 to 29 years ago). A simplified solid model of the Sublimator CHX is provided in Figure 4a with several dimensions noted. The hydrophilic coating promotes film condensation, and capillary connection around the perimeter of the CHX channels assures liquid accumulation along the axial cusp interior corners of the channels[8] as depicted in Figure 4c. We note that favorable wetting does not assure liquid coverage and thus suction access by the slurper holes identified in Figure 4c, which are exploited to withdraw condensate from the Sublimator CHX channels. However, the abrupt ends of the individual CHX channels serve as pinning edges[9] for wetting films that pile up to form annular rings that then back-up upstream eventually covering the slurper holes and allowing for efficient liquid withdraw within the CHX. This description is supported in Figures 4c-f, where in Figure 4d SE-FIT[10] numerical computations display the path to annular channel edge pinning in a simple circular tube as a strong function of increased airflow, liquid volume, and acceleration field strength (i.e., gravity), while a somewhat weak function of wetting conditions. Full scale single channel empirical horizontal terrestrial demonstrations of the phenomena are shown in Figures 4e-f for favorably wetting water with dilute surfactant (anti-fog, Joy Ultra®).

Horizontally-oriented 1:1 terrestrial demonstrations of the CHX slurper approach reveals 100% condensate collection (0% carry-over). This does not guarantee such results in microgravity where condensate hold-up in the CHX, Vent Loop, T2 Port, and Helmet Vent Pad can be significant yet not escape into the helmet for observation during an EVA. Observations of the irregular pinning edges around the CHX channel perimeters (ref. Fig. 4a-b) suggest that conduit faces flush with the downstream manifold ceiling provide little if any pinning allowing irregular annular menisci that are likely to weep into the Vent Loop with increased hold-up leading to increased local airflow velocities. Poor wetting can also lead to bypassed slurper holes as well as ‘plugged’ slurper holes via stable bubble point conditio. Furthermore, degraded wetting that might be expected due to coating fouling, flaking, and cracking can lead to dropwise condensation, increased CHX hold-up, and stick-slip capillary flows in the CHX channels which, if even partially occluding, can be intermittently propelled by the airflow past the slurper holes and into the downstream plumbing. All such ill-effects are exaggerated with increased condensate water production. By such mechanisms is water condensate capable of escaping the CHX and migrating downstream in the direction of the Helmet.

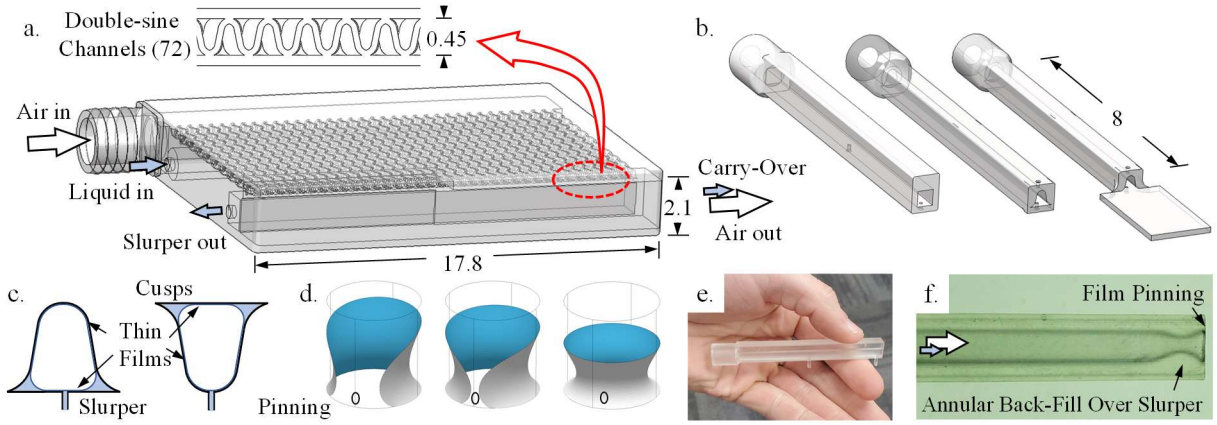

Figure 4. 1:1 Sublimator CHX model with demonstrations of capillary behavior within channels: a. doubly-sinusoidal Sublimator CHX channels (dim. in cm) with simulator flows identified, b. example solid models of single channel types with slurper holes and pinning configurations (square, sine, and poorly pinned sine), c. channel end section identifying thick cusp and thin film regions for right side up and upside down channels, d. SE-FIT[9] numerical predictions of pinning, annulus formation, and back-fill mechanism that eventually covers the slurper hole despite variations in wetting, e. image of straight 1:1 scale single SLA CHX channel with sections in b., and f. top view terrestrial demonstrations using channel in e. (note: covered slurper hole underneath not visible).

III. Requirements

Due to the urgency of the situation, the non-zero likelihood of water in the helmet forced informative analyses, visualizations, and mitigation efforts beginning with the helmet and ending with the upstream plumbing. Key requirements for the investigation include: (1) Understand fluid behavior of free water inside the Helmet, T2 Port region, upstream plumbing, and CHX source, (2) Conduct analyses for pertinent wall-bound droplet and rivulet flows throughout the system including predictions of liquid hold-up and stability, (3) Establish and demonstrate leak hazard mitigations, (4) Establish materials of construction and critical performance properties, (5) Establish methods to capture and contain water before it enters the helmet, (6) Verify and validate the safety and effectiveness of near-term solutions through computational analyses of helmet-bound water, destabilizing g-levels, and scaled terrestrial measurements and demonstrations, (7) Verify and validate via ISS measurements and demonstrations, and others. We address such requirements as applied to the Helmet, T2 Port region and water capture device, Vent Loop, Sublimator CHX source, and integrated system.

IV. Helmet

The instances of significant water in the Helmet (ref. Figure 2) reveal unearthly large Helmet-bound drops interspersed and fed by smaller Helmet-bound rivulets, the latter which thin and rupture into trains of temporarily stationary helmet-bound droplets. Both Large and small Helmet-bound drops inch their way downstream along developing airflow streamlines. The motion of such drops is governed by the local Weber number, $We \equiv \rho U_a^2 D/\sigma \gtrsim 4$, from which it is observed how larger coalescing drops are easier to move in faster air. Such flows are inherently unsteady and arise in systems with low liquid-to-gas flow rate ratios $Q_l/Q_a << 1$ with poorly and partially wetting walls with contact angles $40° \lesssim \theta \lesssim 80°$ with large hysteresis ~ ± 20°. A selection of sketches of mechanisms and fluid interface configurations are provided in Figure 3. Expected outcomes are strongly wetting-, volume-, and geometry-dependent.

Figure 3a-d illustrates the process of transition for a coalescing wall-bound drop to a transient rivulet and then to a train of wall-bound drops. Figure 3e-h depicts a similar process for a slug through film pulling, slug rupture, film rupture, and then to a train of wall-bound drops. Figure 3i provides a sketch of related expectations in the helmet. Static[10] and dynamic numerical[11] tools may be applied to determine the stable configurations of large droplets that bridge helmet and head/face. Sample results are shown in Figure 5a using a contact angle regime map and in Figure 5b for an example of computed droplet transfer dynamics. The expected domain of the helmet is indicated by the dashed rectangle in 5a, where it is observed that the stable concave bridge is the most likely configuration to arise.

Such bridges are unstable to sufficiently perturbations and local capillary draining leading to possible liquid transfers to the head/face, or Helmet, or both.

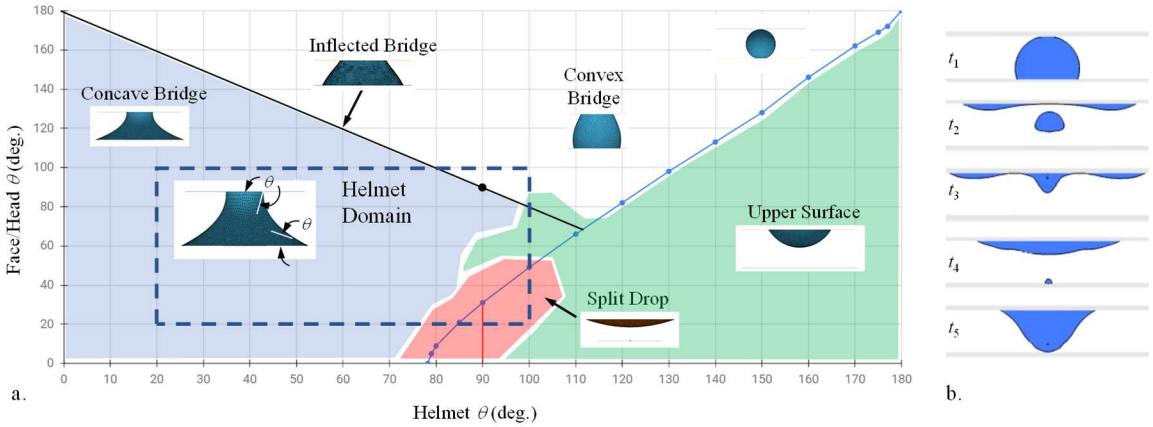

Figure 5. a. Static SE-FIT[9] and b. dynamic Basilisk[10] computations of static interface configurations for large droplets between Helmet and face/head. Largely stable concave bridges are formed in the Helmet domain identified by dashed region in a.

A. Scaled Terrestrial Model

Though certain Helmet flow phenomena may be anticipated qualitatively, quantitative predictions are challenged by the large-scale nature of the unsteady, undeveloped, and transitional inertial-visco-capillary two-phase microgravity flow of a variable poorly wetting liquid in a complex geometry with unknown initial conditions in an uncontrolled perturbation environment[12]. In the absence of sufficient analytical or numerical tools to model such complex flows on short order, empirical terrestrial scale model demonstrations are pursued. To minimize the impact of gravity, a 2D projected capillary-dominated scale model of the Vent Pad and Helmet flow was quickly developed to evaluate flow regimes as functions of inlet conditions and confirm or deny our qualitative expectations of on-orbit behavior. In an attempt to best mimic the flow regime along the Helmet, we choose to match the area-averaged Weber number along the Vent Pad exit ports with the scaled terrestrial model (note: Reynolds number does not match). To begin the process, full-scale full-3D single-phase airflow CFD computations[13] within the helmet are conducted to determine average Vent Duct velocity vectors along the Vent Pad. These values are sketched in Figure 6a for the EVA airflow conditions of $Q_a = 6$ acfm at $P = 4.3$ psia). Local Weber numbers $We_i \sim (\delta U^2)_i$ are computed and area-averaged to find δU^2 for the entire Vent Pad, where δ is the Vent Pad depth (≈ 9 mm at the T2 Port). We then compute the scale channel depth δ_{scale} to minimize (maintain) gravity (capillary) effects where $Bo \lesssim 1$, such that $\delta_{scale} \lesssim (\sigma/\rho_l g)^{1/2}$. We choose $\delta_{scale} \approx 3$ mm for our fluid (water) properties, establishing device scale ratio $\delta_{scale}:\delta \approx 1:3$ at the T2 Port location. We then equate $\delta U^2 = (\delta U^2)_{scale}$ and solve for U_{scale}, then Q_{scale}, $V_{scale} \approx (\delta_{scale}/\delta)^3$, etc.

The 1:3 scaled model is projected onto a horizontal plane for 2-D similitude. Solid model drawings and an image of the transparent SLA part are provided in Figure 6b-c, with sample test results shown in 6d. The schematic section of Figure 6e provides further details of the 1-g horizontal Helmet leak test analog. Sample test results are shown in Figure 7. For the comparable model test conditions of $Q_a = 1.5$ cfm at 14.7 psia, the impact of liquid flow rate/volume is shown in Figures 7a-c for five 1 mL injections (7a), four 5 mL injections, and four 1 mL injections over a helmet model with anti-fog coating within the black dashed region. Such water injections are equivalent to 30, 120, and 24 mL injections for the full-scale system, respectively. From Figure 7c it is clear how the water dissolves the coating, reduces its contact angle, and spreads thinly in all directions. Figure 7d-i demonstrates the absorption rate and capacity for a HAB-like mitigation to be described in further detail shortly.

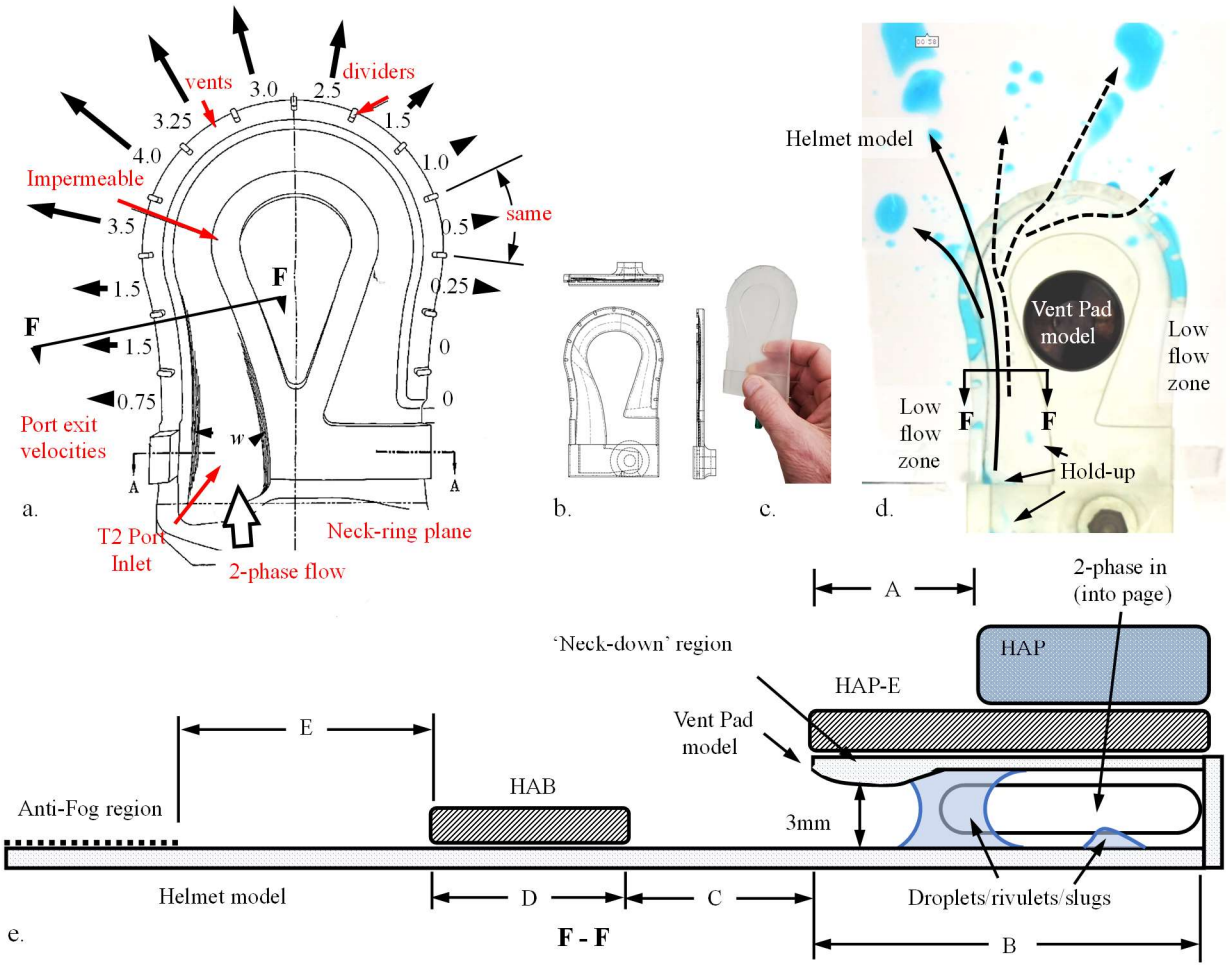

Figure 6. Terrestrial Helmet model items: a. Rear view of Vent Pad with average Vent Duct velocities sketched from CFD computations, b. Solid model views of planar-projected Vent Pad 1:3 scale model (to scale with a.), c. Image of model (to scale with a.), d. Top-down view of sample 1-g horizontal test showing wall-bound rivulet (solid) and droplet (dashed) pathlines. e. Schematic section F-F of scale model identifying 2-D horizontal Vent Pad and Helmet models. Scale model versions of mitigations HAP, HAP-E, and HAB are labeled along with geometric layout test parameters A, B, C, D, and E.

B. Helmet Mitigations

Three water leak mitigations are employed within the helmet as identified in Figure 8: the Helmet Absorption Pad (HAP), the HAP-Extender (HAP-E) and the Helmet Absorption Band (HAB). The HAP consists of a Tranquility fabric-covered absorb-and-lock gel material (i.e., diaper gel). The HAP is attached to the inner surface of the Vent Pad which contacts the perfectly wetting Comm Cap covering the head of the crewmember, ref. Fig. 3i-l. The HAP was first implemented during Expedition 38, EVA-24, December 21, 2013 with Astronauts Rick Mastracchio and Mike Hopkins. Despite a holding capacity of ≈ 800 mL, early demonstrations of the HAP proved somewhat ineffectual due to its limited capillary reach and the fact that large liquid inventories leaking into the helmet are deposited elsewhere and are slow to establish a capillary connection to the HAP. The HAP-E adds a 2 mm thick wetting 100% Rayon Felt layer beneath the HAP, extending the reach of the HAP just short of the Vent Pad exit ports per safety limitations.

Helmet-bound drops and rivulets propelled beyond the Vent Ducts impact, wet, and are wicked and stored by the HAB, a 2 mm thick Rayon Felt strip adhered to the inner surface of the helmet in the manner of a halo (aka 'Luca Halo'). Provided the water injection rate and overall volume are low enough, the HAB is capable of its complete absorption, preventing excess water migration across the helmet obstructing crew visibility. Once saturated, the HAB

provides a superhydrophilic region allowing further water accumulation super-saturating the HAB. In the event of overwhelming water injection, the HAB also serves as a significant capillary flow resistance element, backing-up Helmet-bound water with increased likelihood of capillary connections with Vent Ducts, then HAP-E, then HAP, or even to Comm Cap, then HAP.

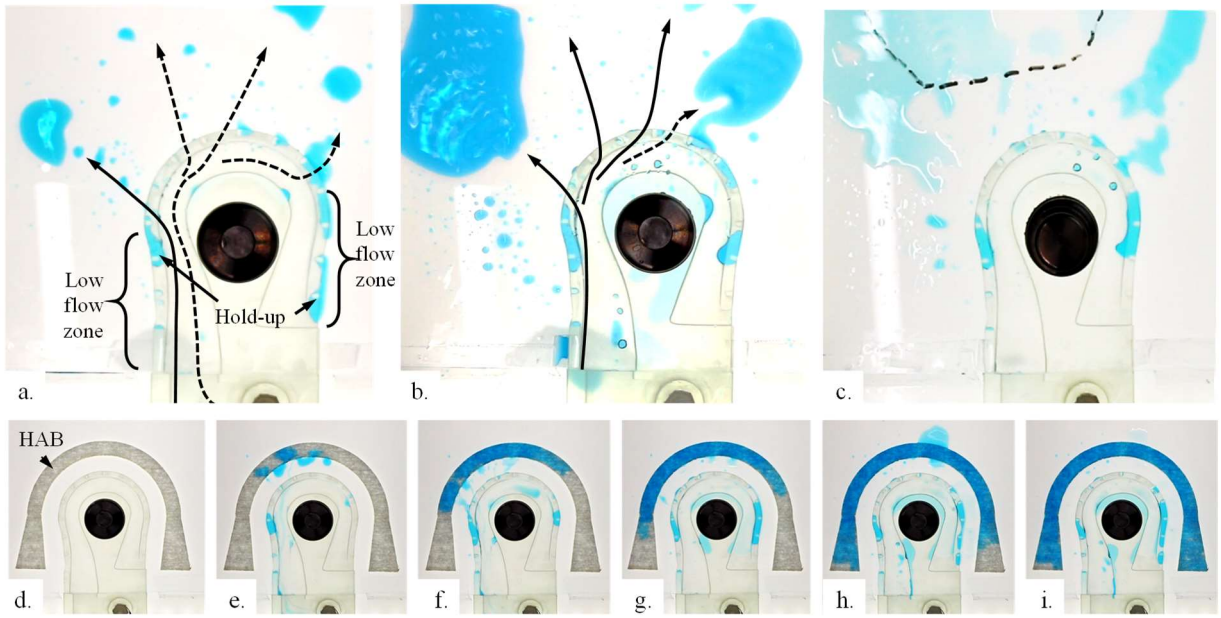

Figure 7. Terrestrial Helmet model demonstrations: a. Trickle flow five 1 mL injections (equiv. 6 mL injections, total 30 mL), Pulse flow four 5 mL injections (equiv. 30 mL injections, total 120 mL), c. Trickle flow four 1 mL injection (equiv. 6 mL injections, total 24 mL) with anti-fog region identified in black dashed region, and d.-i. demonstrations of HAB-like mitigation at approximate flow conditions of a.

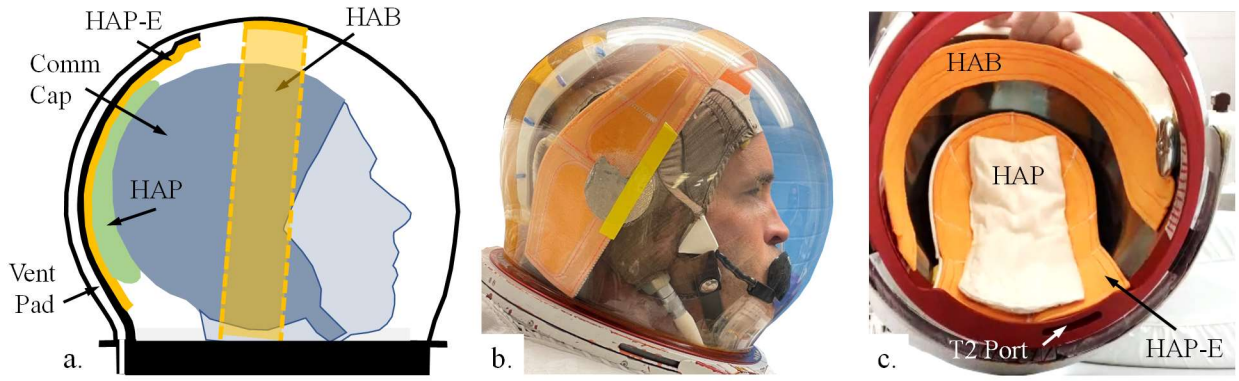

Figure. 8. Helmet mitigation: a. sketch of HAP, HAP-E, and HAB, and images b.-c. of side and bottom views of early prototypes. The Comm Cap provides an additional parallel wicking path to the HAP.

HAB demonstration tests were conducted using the terrestrial model discussed in connection with Figure 7. In Figure 7d-i it is observed how the HAB functions to wick, distribute, and hold injected water. In Figure 7h, a several second pulse injection temporarily overwhelms the local wicking rate of the HAB but is eventually and completely absorbed by the HAB. Concepts to attach HAB to HAP-E via Rayon Felt 'straps' at the base of the HAB halo were successfully demonstrated but not implemented in the flight mitigations.

The HAP-E and HAB mitigations depend on the capillary performance of the wicking material (i.e., Rayon Felt). Felt porosity ($\epsilon \approx 0.95$), bubble point (≈ 735 Pa), Jurin height (≈ 75 mm), effective pore size ($r_p \approx 180$ µm) and transient wicking rate coefficients were measured, the latter by conducting horizontal wicking tests for 2 mm thick 20 mm wide

Rayon Felt strips laying on a super-hydrophobic tabletop to find flow rate $Q(t) = \epsilon A(k\sigma r_p/\mu t)^{1/2}$ and volume storage rate $V(t) = 2\epsilon A(k\sigma r_p t/\mu)^{1/2}$, where A is the felt cross-flow area and $k \approx 0.0072 \pm 0.0020$ is a dimensionless empirically-determined flow resistance coefficient. Depending on contact area, we note that initial nominal Rayon Felt HAB absorption rates are as high as ~ O(10 mL/min) for water with absorption capacity ~ O(100 mL). Estimated stable low-frequency (<< 1 Hz) accelerations to an under-saturated HAB are in the neighborhood of $a \sim \sigma/\rho_l r_p L_{HAB} \approx 0.2$ m/s^2 ($\approx 2\cdot10^{-2}$g), while for a saturated HAB $a \sim \sigma/\rho_l w_{HAB} L_{HAB} \approx 0.03$ m/s^2 ($\approx 3\cdot10^{-3}$g). The total absorption volume of the helmet mitigations HAP (≈ 800 mL), HAP-E (≈ 150 mL), and HAB (≈ 75 mL) are expected to be $V_{tot} \approx 1000$ mL.

C. ISS Demonstrations

HAP, HAP-E, and HAB mitigations were rapidly adapted to the helmet and launched to ISS on Crew-4 April 25 2022 (-702), OFT-2 May 21(-703), and SpX-25 July 15 (-705, -706), 2022. The demonstrations were performed May 20, 22, and 26, 2022 (EVA Flow and Swish Tests). Crew procedures were established for critical engineering demonstrations including > 50 mL isolated dry (slow) and pre-wetted (fast) HAP and HAB wicking tests, integrated water-helmet flow tests, wall-bound droplet and rivulet flow and stability tests within the helmet, and an approximately 250 mL/min water absorption test in contact with a donned Comm Cap. Figures 9 and 10 provide a selection of images highlighting the tests performed. The first set of tests (Test OpNom EVA-1) were completed by Astronauts Samantha Cristoforetti and Kjell Lindgren May 2, 2022 and focused on two-phase flows, liquid configurations, and stability within an empty helmet. The second set of tests (Test OpNom EVA-2) were completed by Samantha Cristoforetti, Bob Hines, and Jessica Watkins May 26, 2022, which focused on mitigations. The ISS experiments were performed on the MWA in Nodes 1 and 2 employing the hotwire anemometer-calibrated 'elephant trunk' duct for airflow. The findings are only summarized herein with test details to be reported in a subsequent publication.

Test OpNom EVA-1. Flow tests were completed with nominal ≈ 1.5 cfm airflow at P = 14.7 psia through the T2 port into an empty helmet with successive water injections of 20, 40, and 80 mL (140 mL total). Capillary liquid occlusions around the vent pad were observed, which led to increased wall-bound liquid escaping across the inside of the helmet with increased liquid volume introduced (ref. Fig. 9h). Large surface deflections and even large bursting bubbles were observed resulting in part from the low airflow rate and low surface tension due to dissolution of the antifog coating and back-wetting upstream towards the Vent Pad. As noted by the crew, the head of a crew member would certainly interfere with such occurrences. Tests to establish helmet-bound water stability were conducted for a critical range of helmet-bound drops (5, 20, and 80 mL) with and without the antifog coating on the helmet. The manually-imparted perturbations reveal static and dynamic advancing and receding contact angles, natural frequencies, sliding stability limits, rivulet pulling limits, and drop break-up limits with accurate measures of break-up volumes. Deflections are measured to predict perturbation levels leading to bridging between the helmet and head. This data cannot be replicated in terrestrial tests. Unique effects of the spherical geometry of the helmet were observed where droplets ejected from break-up reattach to the Helmet readily and immediately. The flight footage confirms the static, dynamic, and stability behavior of such large helmet-bound liquid bodies and serves as a design guide for the mitigations development effort.

Test OpNom EVA-2. For the mitigation tests, the crew performed an installation of the HAP, HAP-E, and HAB in the EMU Helmet on orbit. Empty Helmet (no crew head) flow tests at approximate EVA airflow conditions ($Q_a \approx$ 1.5 cfm at P = 14.7 psia) were then repeated, incrementally increasing the amounts of water injected into the T2 Port (20, 40, and 80 mL). The Helmet-bound water moved qualitatively as expected along airflow streamlines, accompanied by rivulet ruptures and multiple bubble entrainment and burst events. Helmet-bound water that contacted the HAB remained adhered to it and was absorbed by it, the absorption rate decreasing with increased saturation. Furthermore, due to perfect wetting (water-on-water), a thick layer ~ O(3 mm) of water continued to coalesce and accumulate on the HAB. An example of a temporarily over-saturated HAB is shown in Figure 10, where relaxation of the water flow allows time for the advancing liquid to be wicked backward into the HAB, comparing well with ground test results (ref. Fig. 7h-i).

Perhaps most importantly, the integrated flow tests exploiting ISS cabin airflow matching EVA Reynolds numbers in the Helmet demonstrate the following: the HAB readily and stably wicks Helmet-bound droplets and rivulets. As intended, the HAB redistributes water laterally away from the primary flow path of the air (ref. VD4-VD7 Figs. 2c, Fig. 6a). Additionally, the HAB serves as a wetting 'energy well' for additional liquid and can attract and hold approximately twice its internal capacity. Higher holding capacity, potentially bridging to the crew head/face, appears possible and is limited only by re-entrainment due to airflow and crew perturbations. Stable ~ O(1 Hz) perturbations for the saturated HAB are found to be $\lesssim 10^{-1}$g, while stable perturbations for a super-saturated HAB are found to be $\lesssim 10^{-2}$g.

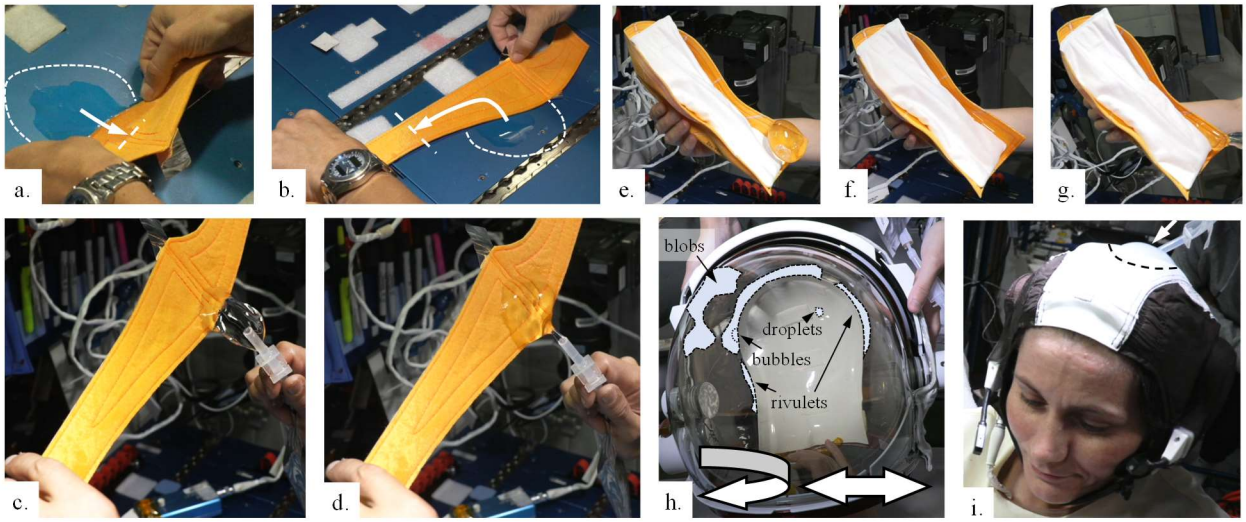

Figure 9. Selection of Helmet mitigation demonstrations on ISS: a. normal and b. lateral wicking tests into HAB element on MWA with water source (within dotted line), wicking direction (solid line), and advancing front (dashed line) noted. c.-d. Water is propelled into pre-wetted HAB within seconds by capillary forces. e. Wicking of 73 mL droplet into dry HAP/HAP-E at $t = 0$ s, complete by f. $t = 45$ s with interior corner wetting indicated. g. Inertial capillary wicking of additional 50 mL into pre-wetted HAP/HAP-E completed in less than 10 seconds. h. Helmet-bound droplets, rivulets, and bubbles arising from 2-phase flow tests in helmet. Quantitative rotational and translational perturbations imparted by crew identified by arrows. i. Within 2 minutes, 250 mL of water is injected and readily absorbed in by the Comm Cap-covered head of ESA Astronaut S. Cristoforetti.

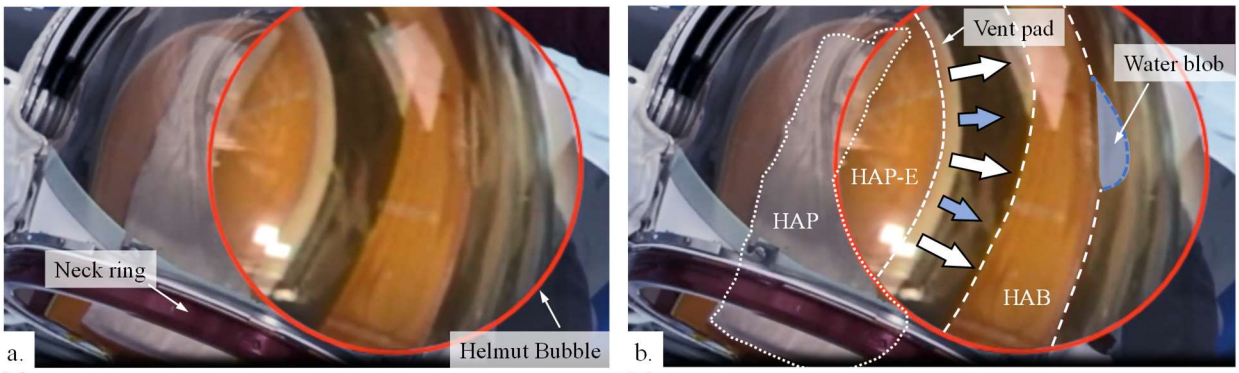

Figure 10. ISS images of HAP, HAP-E and HAB wicking demonstrations: a. image and b. duplicate annotated image. Note large liquid blob in b. advancing past HAB only to be reclaimed by HAB as anticipated in terrestrial scale model tests (ref. Fig. 7h-i).

D. Brief Helmet Summary

In general, the Helmet water mitigations absorb and retain water as expected with initial dry media absorption rates slower than expected (delayed by the slowly wetted edges, sewn seams, adhesive strips, and PFTE reinforcements of the Rayon Felt items) and wetted media absorption rates faster than expected (propelled by inertial-capillary forces). We observe that water wicks from both HAP-E and Comm Cap/Crew head into the HAP quickly and effectively. We find that the HAB provides an effective control against large quantities ~ O(100 mL) of water migrating across the inside surface of the Helmet. We also observe that Helmet-bound water can be moved by relatively small perturbations $\lesssim 10^{-2}$g, and that moderate to large quantities can be liberated from the Helmet surface posing a threat of transfer to the head/face. Again, from the crew we learn that it is difficult for suited or non-suited crewmembers to estimate water quantities and to differentiate water motion from water increase. Lastly, we note that the water behaves as qualitatively anticipated by the terrestrial 1:3 scale model (ref. Figs. 6-7).

V. T2CCS: Passive Water Phase Separator, Ground Tests, ISS Test Plan

Early during the mitigations effort, the T2 Port region of the suit was viewed as a possible location to install, or 'cut in', a passive water separation device to reduce or eliminate the need for mitigations within the helmet. The reverse-engineered Solid Model of the neck and shoulder region of the HUT revealed an irregular though non-negligible volume below the neck ring and above the left shoulder of the crewmember. Numerous designs were pursued, with prototypes fabricated and tested. Only the final design that shipped to ISS for low-g demonstrations is reviewed here with sub-project OpNom T2CCS (T2 Condensate Capture System). The HUT with T2 region identified is depicted in Figure 11a. The open space above the left shoulder to be occupied by the T2CCS is identified in Figure 11b, which is labeled and presented in perspective view in Figure 11c with T2CCS pasted in. Requirements for such a device are stringent and include no moving parts, no blockage or disruption of the flow path, no additional pressure losses, no interference to crew mobility, and material compatibility.

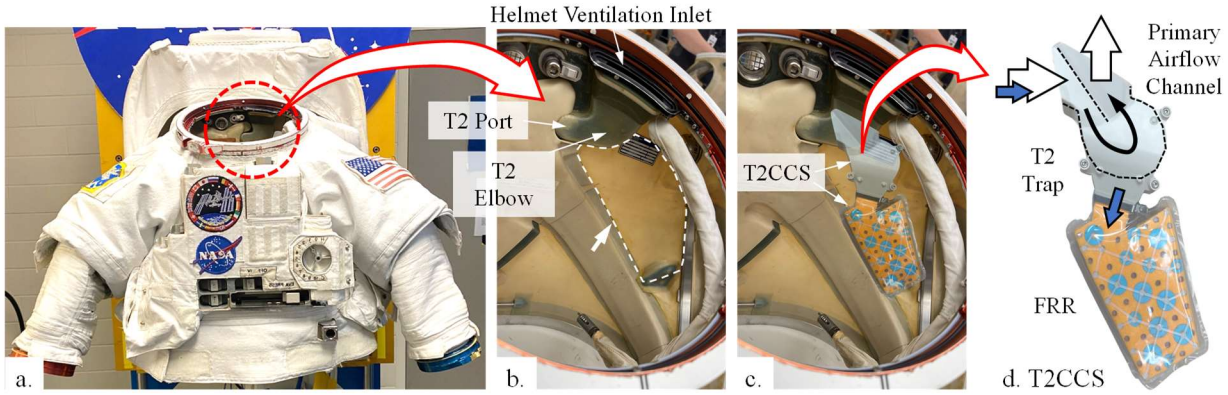

Figure 11. T2 Port Region and T2CCS modification: a. Suit HUT with T2 region identified, b. magnified T2 region with available design volume denoted by white dashed region, c. image of b. with T2CCS superimposed, and d. magnified image of T2CCS prototype with air (white arrows) and condensate (blue arrows) flows indicated (black dotted lines comprise primary airflow channel).

As described in Section II, and in reference to Figure 11d, the two-phase flow regime entering the T2 Port region is a mixed transient undeveloped wall-bound rivulet and droplet flow, with intermittent free droplets emitted near irregular geometries such as re-entrant corners, pinning edges, etc. The airflow is diverted into the weakly expanding approximately 180° curved elbow containing a 1.2 mm thin 3D printed porous 17-4 stainless steel insert of varying rectangular section called the 'Flow Shaper' (ref. Fig. 12). The rounded slightly expanding nature of the Flow Shaper reduces pressure loss through the device below that of the original T2 Port elbow (ΔP_{elbow} = 0.25 in. H_20). The 'top' and 'bottom' faces of the Flow Shaper are overlain with 2 mm thick Rayon Felt sheets that extend past the flow shaper sandwiching a stack of up to 4 Rayon Felt sheets forming a capillary-connected wick layup that extends to a wick reservoir (ref. Fig. 11d and 12). During operation, wall-bound water pins at the Flow Shaper edge, eventually saturating the poorly wetted pores ($\theta_{17\text{-}4} \approx 70° \pm 30°$). Capillary connection between the Flow Shaper and Rayon Felt is made and the liquid is effectively wicked away from the Flow Shaper channel, into the body of the separator, and down to the Flexible Retention Reservoir (FRR). The T2CCS water storage capacity is 28.2 mL and the FRR adds approximately 200 mL (228 mL total T2CCS capacity). The FRR is constructed of flexible heat-sealed polyurethane with distributed rigid inserts to prevent compression due to crewmember shoulder motion. The reservoir employs an air bleed port capable of weeping liquid in the event the ≈ 228 mL capacity of the device is exceeded.

The approximate limits of operation of the device are established via horizontal terrestrial tests at EVA and IVA airflow conditions under a variety of expected water injection rates and rate profiles. The experimental set-up and typical results are shown in Figure 12 where blue-dyed water makes saturation level obvious. For EVA conditions with Q_a = 1.5 cfm, we find ΔP = 0.186 ± 0.004 (in. H_2O) for a maximum steady liquid uptake rate of $Q_l \approx$ 2 mL/min with no observed water carry-over. At this rate it requires approximately 15 min to partially saturate the device and begin wicking water into the reservoir. We also find maximum pulse injection limits of 8 mL in 60 s, 4 mL in 30 s, and 3 mL in 10 s. Microgravity operation of the device will be enhanced by uniform wicking around the Flow Shaper, but retarded by the absence of a gravity siphon effect within the felt present in the terrestrial tests. Neither of these effects are expected to impact the airflow pressure drop results. In the case of IVA flow Q_a = 6.0 cfm and we measure

ΔP = 1.2 ± 0.1 in. H_2O. The stability of the liquid captured by the device is high and perturbations $\lesssim 2 \cdot 10^{-1}$g are incapable of releasing stored water.

The T2CCS is scheduled to fly to ISS April – August 2023 for integrated testing with the upstream EGS as sketched in Figures 13 and 14. The combined effort is named the T2 And Ventilation Visualization ISS Demonstration (TAVVID). In a similar manner to the terrestrial tests, for EVA airflow, water will be injected into the EGS until the maximum hold-up capacity is reached. Further water injections will result in carry-over from the EGS to the T2CCS, the volume of which will guide microgravity hold-up estimates as coarsely pursued herein. Manually-imparted perturbations to the assembly by the crew will provide a second method of liquid release from the EGS into the T2CCS. HD video images of the events will serve as quantitative measures to assess the performance of this T2 Port water capture mitigation.

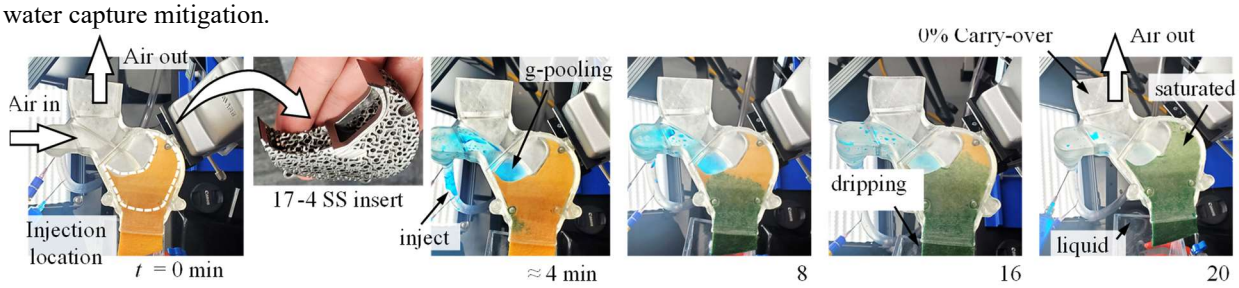

Figure 12. T2CCS testing: Top-down view of terrestrial performance tests with white dashed region identifying 3D printed 17-4 SS flow shaper insert and subsequent series of images during ≈ 20 min of injections: 40 mL total injection, excess liquid observed at 16 min, 28.2 mL local capacity, max. water separation rate is 2 mL/min with 0% carry-over. Gravity effect identified at $t \approx 4$ min.

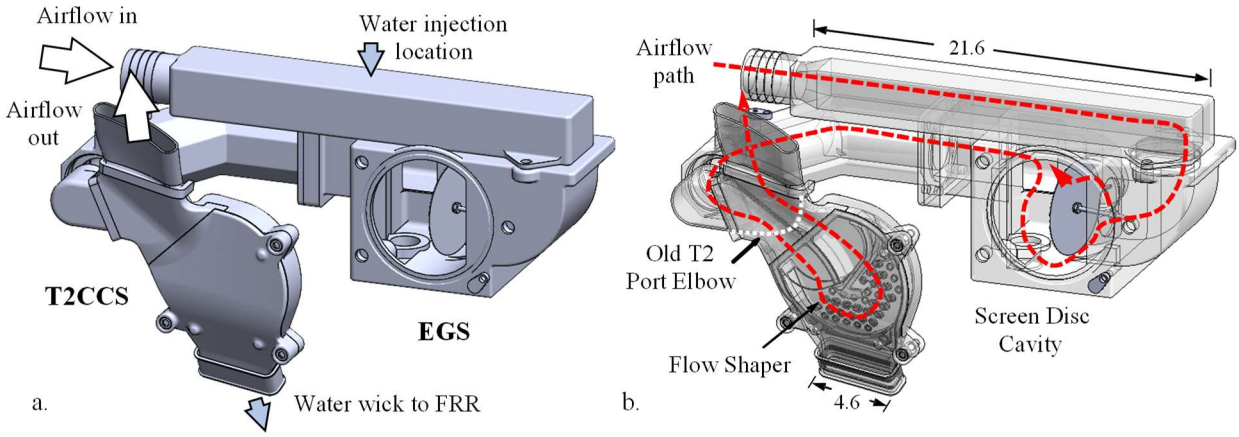

Figure 13. Integrated EGS and T2CCS Assembly: a. Opaque and b. translucent solid models. Airflow path disc cavity and Flow Shaper, and select reference dimensions (cm) identified in b.

VI. EGS: Hardware, Hold-Up Analysis, ISS Test Plan

A solid model of the Vent Loop plumbing element just upstream of the T2 Port region and just downstream of the Sublimator CHX is shown in Figures 13 and 14. The reverse-engineered 1:1 scale EGS model receives simulated CHX condensate carry-over water from the water injection port (not pictured). Wall-bound drops and rivulets dominate the downstream two-phase flow[14,15] due to poor wetting materials. From the dimensions provided, local duct Weber numbers employing local cross-section-averaged airflow velocities are used to estimate minimum water hold-up volumes in each element of the Vent Loop (EGS): Downstream Manifold, Horn, Screen Cavity, annular passage within the screen cavity, and Downstream Leg. The calculations assume that liquid will hold-up where $We_D \equiv \rho_a U^2 D/\sigma \leq 4$. In each conduit section, a wall-bound droplet (assume $\theta \approx 90°$) increases in volume with increased coalescence. As the droplet increases in size the conduit becomes increasingly occluded increasing the average velocity U of the incompressible airflow around the drop. At some point the increasing droplet size and airflow velocity achieve $We_D \geq 4$ and the droplet is destabilized and driven further along and/or out of the conduit. In an average sense, these conditions are governed by

$$Q_a = U(A - A_D) \quad (1)$$

and

$$4 \approx \rho_a U^2 D/\sigma, \quad (2)$$

where Q_a is the known airflow rate, A is the known crossflow duct area, and the wall-bound drop projected area is $A_D = \pi D^2/8$. Air velocity U and wall-bound droplet diameter D are unknown. Introducing dimensionless airflow velocity $U^* = AU/Q_{air}$ and dimensionless constant $A^* = 2\pi\sigma^2 A^3/\rho_a^2 Q^4$, writing eq (1) in terms of U^* yields the 4th-order polynomial

$$U^{*4} - U^{*3} - A^* = 0, \quad (3)$$

which is solved for the single real positive root, where $U^* = U^*(A^*) \geq 1$ is the decimal percent increase of the airflow velocity due to the occluding wall-bound drop. For each section of the EGS, A^* is computed, then U^* solved from eq (3), then $U = QU^*/A$ is found and employed to compute hold-up droplet diameter D from eq (2). With D thus estimated, a solitary wall-bound water droplet hold-up volume

$$V_{hu} \approx \pi D^3/12 = (16\pi/3)(\sigma A^2/\rho_a Q^2 U^{*2})^3 \quad (4)$$

may be estimated in the various sections of the EGS as well as the Helmet Vent Pad, Sublimator CHX, etc. Approximate limiting solutions to eq. (3) are

$$U^* = 1 + A^* - 3A^{*2} + O(A^{*3}) \quad (5)$$

and

$$U^* = A^{*1/4} + 1/4 + O(A^{*-1/4}). \quad (6)$$

Equation (5) is accurate to < 5% for high airflow limit $A^* \leq 0.2$ and eq (6) is accurate to < 5% for low airflow limit $A^* \geq 3.6$. We also note alternatively that $A^* = 2\pi/We_{duct}^2$, where $We_{duct} \equiv \rho_a Q^2/\sigma D_{duct}^3$ and $D_{duct} = A^{1/2}$.

A 1:1 scale Transparent SLA printed EGS is scheduled to fly to ISS along with the T2CCS as part of TAVVID during the April – August 2023 timeframe. Integrated tests of the EGS with the T2CCS will be pursued as briefly discussed in Section V. A solid model assembly of the flight hardware for integrated tests on the MWA aboard ISS is shown in Figure 14. The figure includes EGS, T2CCS, and a Water Trap to capture carry-over water escaping the T2CCS while allowing the airflow to vent into the cabin. Portable light panels illuminate a diffuse screen providing backlighting for the primary camera view identified on the MWA.

VII. EMU Sublimator CHX and Calibration Hold-Up Demonstrations

The EMU Sublimator CHX is considered the primary source of Helmet water in this paper. The specific condensate channel/slurper hole geometry approach employed was discussed in Section II. Terrestrial test stand performance of the EMU CHX at the time of manufacture (circa 1975-1982) demonstrated excellent 100% collection for a water condensation rate of approximately 1.5 – 3 mL/min. Such results could have been enhanced by the presence of gravity, but they are certainly aided by the highly favorable wetting conditions of the freshly applied hydrophilic coating to the CHX at that time. The degradation of these coatings with use could lead to retarded slurper performance and increased carry-over and alternative designs might provide adequate performance without such surface wetting sensitivities. Combined with the flight demonstrations planned for EGS and T2CCS, simple tests of several individual sublimator CHX-type channels are also pursued. Example images are shown in Figure 15 for these Sublimator Test Units where 1:1 scale models are employed to clearly visualize the pinning, slurping, and carry-over of a limited variety of channel sections in the microgravity environment.

The Sublimator Test Units include doubly-sinusoidal channels akin to the current EMU CHX. Half of the channels (36 ea) terminate with sharp (good) pinning edges while the other half terminate with mixed (poor) pinning edges (ref. Fig. 15). Duplicate versions of the test units are provided for favorable (anti-fog coated) and unfavorable (uncoated) wetting conditions. The units apply $D \approx 600$ μm slurper holes whereas the EMU Sublimator CHX slurper holes have $D \approx 280$ mm.

The demonstrations will be performed in like manner to those of TAVVID. The test unit will be set-up on the MWA in the manner of Figure 17a. The airflow will be connected and liquid injected by syringe at locations indicated in Figure 15a-c. The slurper holes will be engaged by withdrawing air and water via syringe as indicated. Visualizations of the channel hold-up performance as functions of liquid inlet flow rate and wetting conditions will provide confirmation or refutation of expectations of CHX carry-over rates and mechanisms. For example, channels flush with the downstream manifold surface will be scrutinized for uneven pinning and weeping. Fluid surface stability will also be assessed through perturbations induced by the crew.

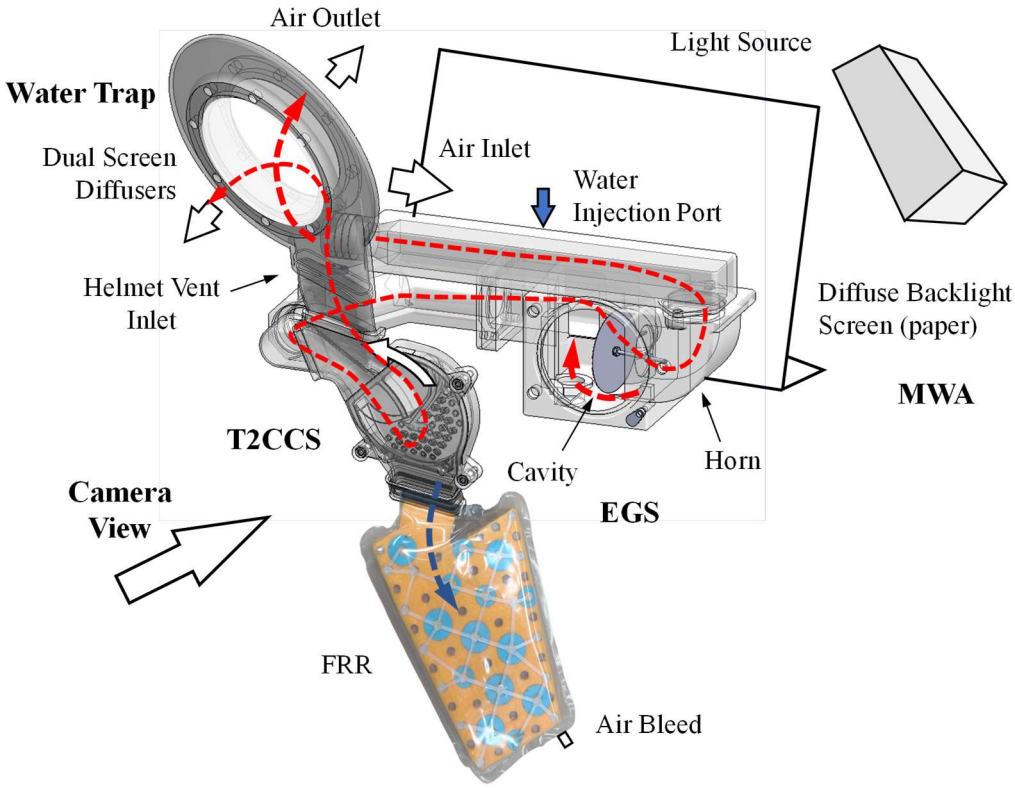

Figure 14. Integrated EGS and T2CCS on MWA: 1:1 Transparent SLA printed EGS with critical components labeled, including airflow path (red dashed lines and white arrows) and water flow path (blue dashed line and arrows). Note that the EGS models the Vent Loop and that the T2CCS replaces the T2 Elbow for the ISS demonstrations. A cyclonic water trap prevents carry-over liquid from exiting into the cabin.

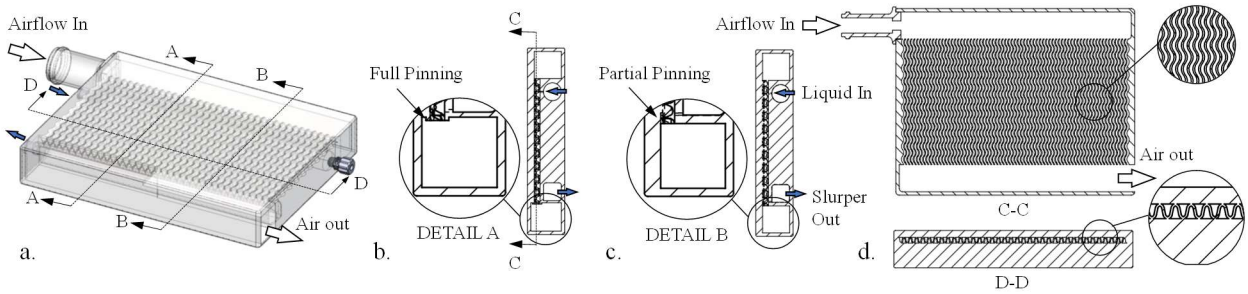

Figure 15. Sublimator Test Unit (CHX Hold-up Demonstrator): a. Solid model, b. section identifying channel exit full (good) pinning detail, c. partial (poor) pinning detail, and d. 72 doubly-sinusoidal channel detail. Two units are provided possessing favorable and unfavorable wetting conditions. Slurper holes $D \approx 600$ µm not shown.

Two Flow Calibration Test Units will be similarly tested. A solid model is provided in Figure 16. The set-up and test procedure for these units is like that of the Sublimator Test Units and as depicted in Figure 17b. Hold-up will be observed and measured for the foundational variety of conduit geometries represented along the serpentine pathway (square, circle, bends, contractions, expansions, manifold, an asymmetric section, and others). The quantitative measure of critical volumes is expected to provide a benchmark dataset for predictions in current and future vent loop plumbing. Duplicate versions of the Flow Calibration Test Units are also provided for favorable (anti-fog coated) and unfavorable (uncoated) wetting conditions.

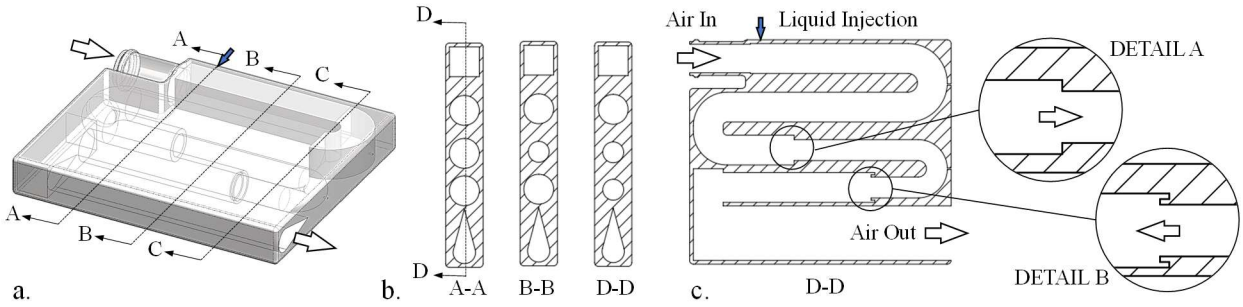

Figure 16. Flow Calibration Test Unit (Calibration Hold-up Demonstrator): a. solid model and b.-c. section detail. Two units are provided possessing favorable and unfavorable wetting conditions.

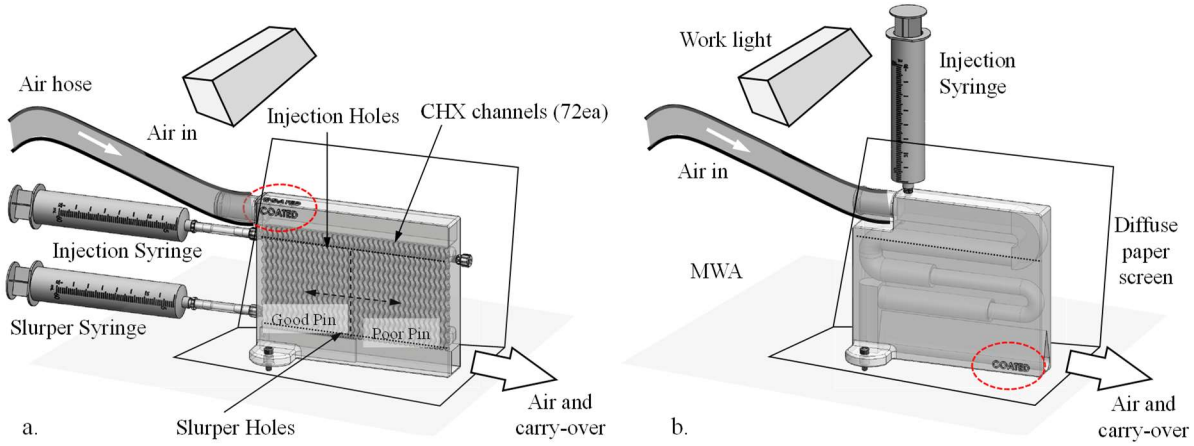

Figure 17. Set-up of a. the Sublimator and b. Flow Calibration Test Units on MWA for ISS demonstrations.

VIII. Summary and Outlook

The EMU EVA Helmet water leak mitigations reported herein are on pace to meet the project requirements to provide understanding and analyses of the unique microgravity fluid behavior, establish and demonstrate leak hazard mitigations, and verify and validate all via ISS measurements and demonstrations for both EVA and IVA conditions. Specific analyses and mitigations are developed and reported for the Helmet, T2 port region, and Vent Loop, with an additional first-ever effort to visualize microgravity EMU Sublimator CHX performance. Successful tests aboard the ISS are completed for the combined Helmet mitigations HAP, HAP-E, and HAB, where we observe the nature of the Helmet-bound droplet/rivulet two-phase flow, the increased likelihood of water transfers to head/face with increased water release, the change in flow configurations when water encounters the antifog region, and the difficulty of visually estimating increasing liquid volumes within the helmet. We observe the rapid absorption of the HAB, which significantly resists if not prevents water from moving beyond the HAB towards the visor obscuring crew vision. The HAB absorbs and holds-up as much as twice its internal volume (> 100 mL) and backs-up the water increasing capillary connections with well-wetting HAP-E and HAP for a combined absorption of ≈ 1000 mL. Demonstrations on ISS reveal the Astronaut Comm Cap is also readily capable of absorbing an additional 250 mL, while transferring significant liquid to the HAP.

The hardware and ground tests for the T2CCS passive liquid separation device and upstream EGS are described along with plans for integrated testing on ISS mid-2023. Terrestrial experiments performed on the down-selected full-scale T2CCS reveal 100% liquid separations for water leak rates $\lesssim$ 2 mL/min for as much as 228 mL. Up to two-fold higher separation rates are anticipated in the low-g environment. A successful T2CCS renders the Helmet mitigations unnecessary.

Wall-bound droplet hold-up is estimated analytically for flows within the Vent Loop upstream of the T2 Port. We currently anticipate $\lesssim$ 100 mL water hold-up within the various sections of the Vent Loop—the screen cavity contributing the lion's share. ISS tests are scheduled for integrated EGS and T2CCS tests where water is injected into the EGS in an incremental fashion to identify Vent Loop hold-up, hold-up stability due to crew perturbations, T2 Port

Hold-up, separation efficiency, and stability to perturbations. Water hold-up within the EMU CHX is also estimated as well as its stability as a function of wetting and pinning edge conditions. ISS demonstrations will confirm or refute all model assumptions employed. It is the water release volume, rate, and character from the Vent Loop that illuminates the true entrance conditions for the T2CCS. It is the water release volume, rate, and character from the T2CCS that illuminates the true entrance conditions for the Helmet.

On Jan. 18, 2023, the EVA and Human Surface Mobility Program (EHP) Mission Implementation Configuration Control Board opted to not continue work on the T2CCS project. While the community acknowledged the technical value and progress of the T2CCS, implementing it on the remaining in-life HUT fleet posed long-term feasibility and risk issues. Because the T2CCS design had matured to the proof-tested flight-fidelity prototype level before this decision, it will be flown to ISS for demonstrations as a downstream element of the TAVVID investigation. Of note, the ability to modify the T2 elbow to install new hardware was demonstrated, significant advances were made developing hardware and procedures for NBL assessments, and fluid flow and stress analyses, ConOps and maintenance procedures, safety documentation, and HUT integration and logistics plans were completed. These will be reported elsewhere.

Acknowledgements

This work was supported by NASA EHP. IRPI was supported in part through NASA SBIR Ph III 80NSSC22CA219 and NASA Contract No. WO-0281 with early insights gained from NASA SBIR Ph II NNX14CJ03C. The authors are grateful for the efficient, insightful, and enjoyable support of the ISS cadre and US and ESA crew: Samantha Cristoforetti, Robert Hines, Kjell Lindgren, and Jessica Watson. We also thank the ground team for hardware development, fabrication, test, and flight qualification support J. Garrison (Jacobs), W. Fritz and E. Bergman (Collins/ESOC), Y. Chen (IRPI), K. Cardin, and B. Conger (Jacobs) for numerical support, and E. Unger and D. Pettit for early HAB concepts and idea stream. We are also indebted to crew testimonies of Luca Parmitano and Matthias Maurer and to crew Chris Cassidy, Karen Nyberg, and Luca Parmitano for early demonstrations of water in the helmet during Increment 35/36 on ISS.

References

[1]National Aeronautics and Space Administration, International Space Station (ISS) EVA Suit Water Intrusion High Visibility Close Call, Mishap Investigation Report, IRIS Case Number: S–2013–199–00005, Date of Mishap: July 16, 2013, Date of Report: December 20, 2013.

[2]Howell, E., NASA shelves routine spacewalks for now due to leaky spacesuit helmet, space.com, October 18, 2022.

[3]Campbell, C., Advanced EMU Portable Life Support System (PLSS) and Shuttle/ISS EMU Schematics: A Comparison, AIAA 2012-3411, 42nd Int. Conf. on Environ. Sys. 15-19 July 2012, San Diego.

[4]Kramer, M., Astronauts Recreate Scary Spacesuit Leak In Orbit (Video), space.com, August 28, 2013

[5]Shepard, L.F., G.P. Durney, M.C. Case. A.J. Kenneway, III, R.C. Wise, D. Rinehart, R.J. Bessette, R.C. Pulling, SPACE SUIT, United States Patent No. 3,751,727, Aug. 14, 1973.

[6]Barajas, A.M., Panton, R.L., The Effects of Contact Angle on Two-Phase Flow in Capillary Tubes, Int. J. of Multiphase Flow, Vol. 19, No. 2, pp. 337-346, 1993.

[7]Clanet, C., Lasheras, J., Transition from dripping to jetting. Journal of Fluid Mechanics, 383, 307-326, 1999.

[8]Concus, P., Finn, R., On the Behavior of a Capillary Free Surface in a Wedge, Proc. Natl. Acad. Sci., 63:2:292, June 1969.

[9]Dyson, D.C., Contact line stability at edges: Comments on Gibbs's inequalities, Physics of Fluids, 31(2):229-232, Feb., 1988.

[10]Chen, Y., B.M. Schaeffer, M.M. Weislogel, G.A. Zimmerli, Introducing SEFIT: Surface Evolver Fluid Interface Tool for Studying Capillary Surfaces, AIAA-2011-1319, 11 pages, 49th AIAA Aerospace Sciences Meeting, 4-7 January 2011.

[11]Popinet, S. (2015), A quadtree-adaptive multigrid solver for the Serre–Green–Naghdi equations. Journal of Computational Physics, 302:336–358, December.

[12]A Midterm Assessment of Implementation of the Decadal Survey on Life and Physical Science Research at NASA, Space Studies Board, National Academies Press, Washington DC. (2018).

[13]Baukus, A., Campbell, C., EMU Helmet Free Water Transport, Assessment for the HAB in Support of EVA 80, 52nd International Conference on Environmental Systems, ICES-2023-431, July, Calgary, 2023. (to appear)

[14]Hooshanginejad, A., Hydrodynamics of Droplets in High-Reynolds-Number Flow Regimes, Ph.D. Thesis, University of Minnesota, May, 2020.

[15]Dimitrakapoulos, P., Higdon, J.J., On the displacement of three-dimensional fluid droplets from solid surfaces in low-Reynolds-number shear flows, J. Fluid Mech. (1998), vol. 377, pp. 189-222.